# Self-dual solitons in a Maxwell-Chern-Simons baby Skyrme model

Rodolfo Casana,[*] André C. Santos,[†] Claudio F. Farias,[‡] and Alexsandro L. Mota[§]
*Departamento de Física, Universidade Federal do Maranhão, 65080-805 São Luís, Maranhão, Brazil*

(Received 8 October 2019; accepted 31 January 2020; published 24 February 2020)

We study the existence of self-dual solitons in a gauged version of the baby Skyrme model in which the Maxwell-Chern-Simons term governs the gauge field dynamic. For such a purpose, a detailed implementation of the Bogomol'nyi-Prasad-Sommerfield formalism provides a lower bound for the energy and the respective self-dual equations. The energy lower bound is quantized because it is proportional to the topological charge of the Skyrme field. Furthermore, neither the magnetic flux nor the electric charge is quantized. We find two types of self-dual Skyrme field profiles: the first is described by a solution which follows a Gaussian decay law, and the second is portrayed by a solution having a power-law decay. For both types of skyrmion profiles, the asymptotic behavior of the respective gauge field is similar to the one for the Abrikosov-Nielsen-Olesen vortices. The localized inversion of the magnetic flux is another feature not observed in other gauged Skyrme models already studied in the literature.

DOI: 10.1103/PhysRevD.101.045018

## I. INTRODUCTION

The Skyrme model [1] is a nonlinear field theory which is originally defined in $(3+1)$ dimensions and whose topological soliton solutions are called skyrmions. It has been a prolific subject in several branches of physics. It is currently understood as an effective field theory for nuclear phenomena describing several hadron and nucleon properties [2], circumventing some technical difficulties present in the underlining quantum chromodynamics. Furthermore, in the realm of condensed matter physics, it has caused exciting research to be applied in the description of some physical systems, such as liquid helium [3], the quantum Hall effect [4], Bose-Einstein condensates [5], chiral nematic liquid crystals [6], magnetic materials [7], and superconductors [8].

The $(2+1)$-dimensional version of the full model [1] is called the baby Skyrme model [9], which is described by the Lagrangian density

$$\mathcal{L} = \frac{\nu^2}{2}\partial_\mu\vec{\phi}\cdot\partial^\mu\vec{\phi} - \frac{\lambda^2}{4}(\partial_\mu\vec{\phi}\times\partial_\nu\vec{\phi})^2 - V(\phi_n). \quad (1)$$

The first contribution is the well-known nonlinear sigma model term. The second term is the counterpart of the Skyrme term in Ref. [1]. The last term, $V(\phi_n)\equiv V(\vec{n}\cdot\vec{\phi})$, is the self-interacting potential guaranteeing the stability of the soliton solutions [10]. The triplet of real scalar fields $\vec{\phi}=(\phi_1,\phi_2,\phi_3)$ represents the Skyrme field, satisfying the constraint $\vec{\phi}\cdot\vec{\phi}=1$, which describes a spherical surface with unitary radius (denoted by $\mathbb{S}^2$). The unitary vector $\vec{n}\in\mathbb{S}^2$ provides a preferred direction in the internal space. The sigma model and Skyrme terms are invariant under $SO(3)$ global symmetry, whereas the potential breaks partially but preserves the $U(1)$ subgroup. Such a potential has a unique vacuum configuration and must satisfy the condition $V(\phi_n)\to 0$ when $\phi_n\to 1$. Although the standard baby Skyrme model describes stable solitons, it does not possess a self-dual or Bogomol'nyi-Prasad-Sommerfield (BPS) structure. On the other hand, in absence of the sigma model term, the so-called restricted baby Skyrme model [11] possesses a BPS structure [12].

A natural physical extension in the study of the baby Skyrme model is the possibility of its coupling to the electromagnetic field in order to investigate their electric and/or magnetic properties. The study of BPS solitons in the gauged restricted baby Skyrme model has already been performed in some cases: the Skyrme field minimally coupled to the Maxwell field [13,14] and the Chern-Simons gauge field [15–17]. In the case in which the Skyrme field is coupled to the Maxwell-Chern-Simons gauge field, the study by means of the BPS technique remains open, but it was performed recently in the supersymmetry context [17].

This paper is devoted to the BPS description of the soliton solutions (and their main features) emerging in a gauged baby Skyrme model in which the Maxwell-Chern-Simons action rules the gauge field dynamic. Our study is

[*]rodolfo.casana@gmail.com
[†]andre_cavs@hotmail.com
[‡]cffarias@gmail.com
[§]lucenalexster@gmail.com

divided as follows. In Sec. II, we present the Maxwell-Chern-Simons restricted baby Skyrme model and the necessity to introduce an auxiliary dynamical field with the aim of gaining a BPS model. The development of the BPS formalism immediately provides the BPS potential, the self-dual equations, and the Bogomol'nyi bound for the total energy. In Sec. III, we restrict our analysis to the study of rotationally symmetric solutions by discussing the boundary conditions and obtaining the physical quantities—namely, the magnetic flux and the electric charge. In Sec. IV, we depict some relevant profiles and discuss their quantitative and qualitative features. In Sec. V, we present our remarks and conclusions.

## II. SELF-DUAL MAXWELL-CHERN-SIMONS BABY SKYRME MODEL

First, we consider a gauged restricted baby Skyrme model in which the Skyrme field is minimally coupled to the Maxwell-Chern-Simons gauge field described by the following Lagrangian function:

$$L = E_0 \int d^2\mathbf{x}\mathcal{L}, \tag{2}$$

where the factor $E_0$ sets the energy scale (which will be taken as $E_0 = 1$ hereafter). The Lagrangian density is

$$\mathcal{L} = -\frac{1}{4g^2}F_{\mu\nu}^2 - \frac{\kappa}{4g^2}\epsilon^{\rho\mu\nu}A_\rho F_{\mu\nu} - \frac{\lambda^2}{4}(D_\mu\vec{\phi}\times D_\nu\vec{\phi})^2 - V(\phi_n), \tag{3}$$

where the coupling between the gauge field and the Skyrme field is given though covariant derivative

$$D_\mu\vec{\phi} = \partial_\mu\vec{\phi} + A_\mu\vec{n}\times\vec{\phi}. \tag{4}$$

The first contribution in Eq. (3) is the Maxwell term, where $F_{\mu\nu} = \partial_\mu A_\nu - \partial_\nu A_\mu$, with $A_\mu$ being the $U(1)$ gauge field, and $g$ the electromagnetic coupling constant. The other contributions, listed in order, are the Chern-Simons term and $\kappa$, its coupling constant, the Skyrme term, and the self-interacting potential $V(\phi_n)$. Also, it will be assumed that all of the coupling constants are non-negative quantities. Moreover, the Skyrme field is dimensionless and the gauge field has mass dimension 1, both coupling constants $\kappa$ and $g$ have mass dimension 1, and the Skyrme coupling constant $\lambda$ has mass dimension $-1$.

To date, no research about soliton solutions obtained from the Lagrangian density (3) has been able to engender a self-dual or BPS configuration. In what follows, we propose a modified version of model (3) supporting a BPS structure.

The corresponding self-dual model is constructed by introducing a neutral scalar field which, besides interacting only with the Skyrme field, also modifies the potential. Such a BPS Maxwell-Chern-Simons baby Skyrme model is described by the following Lagrangian density:

$$\mathcal{L} = -\frac{1}{4g^2}F_{\mu\nu}^2 - \frac{\kappa}{4g^2}\epsilon^{\rho\mu\nu}A_\rho F_{\mu\nu} - \frac{\lambda^2}{4}(D_\mu\vec{\phi}\times D_\nu\vec{\phi})^2 + \frac{1}{2g^2}\partial_\mu\Psi\partial^\mu\Psi + \frac{\lambda^2}{2}(\vec{n}\cdot\partial_\mu\vec{\phi})^2\Psi^2 - U(\phi_n,\Psi), \tag{5}$$

where $U(\phi_n,\Psi)$ is the corresponding potential which is now a function of both $\phi_n$ and neutral scalar field $\Psi$. The term $(\vec{n}\cdot\partial_\mu\vec{\phi})^2\Psi^2$ is gauge invariant because $(\vec{n}\cdot\partial_\mu\vec{\phi})^2 \equiv (\vec{n}\cdot D_\mu\vec{\phi})^2$, but such as the potential, it partially breaks the $SO(3)$ symmetry, preserving only the $U(1)$ subgroup. Furthermore, it is worth mentioning that this term can be expressed as

$$(\vec{n}\cdot\partial_\mu\vec{\phi})^2 = (\vec{n}\cdot D_\mu\vec{\phi})^2 = (D_\mu\vec{\phi})^2 - (\vec{n}\times D_\mu\vec{\phi})^2. \tag{6}$$

Thus, model (5) can be considered a type of Maxwell-Chern-Simons baby Skyrme model due to the presence of the sigma model–like term $(D_\mu\vec{\phi})^2\Psi^2$.

The procedure used to achieve model (5) through the introduction of a neutral scalar field with the aim of attaining a successful implementation of the Bogomol'nyi technique is already well known in the literature. It was first used in the context of Maxwell-Chern-Simons-Higgs models [18] based on supersymmetry (SUSY) requirements [19]. A similar approach has also been successfully implemented in other investigations, e.g., in Refs. [20,21] and in some Lorentz-violating scenarios [22–24].

The equation of motion of the gauge field reads

$$\partial_\sigma F^{\sigma\mu} - \frac{\kappa}{2}\epsilon^{\mu\alpha\beta}F_{\alpha\beta} = g^2 j^\mu, \tag{7}$$

where $j^\mu = \vec{n}\cdot\vec{J}^\mu$ is the conserved current density with

$$\vec{J}^\mu = \lambda^2[\vec{\phi}\cdot(D^\mu\vec{\phi}\times D^\nu\vec{\phi})](D_\nu\vec{\phi}). \tag{8}$$

For the Skyrme field, we obtain

$$D_\mu\vec{J}^\mu = -\left\{\lambda^2\partial_\mu[(\vec{n}\cdot\partial^\mu\vec{\phi})\Psi^2] + \frac{\partial U}{\partial\phi_n}\right\}(\vec{n}\times\vec{\phi}), \tag{9}$$

while for the neutral scalar field results

$$\partial_\mu\partial^\mu\Psi - \lambda^2 g^2(\vec{n}\cdot\partial_\mu\vec{\phi})^2\Psi + g^2\frac{\partial U}{\partial\Psi} = 0. \tag{10}$$

Our effort will be focused on the study of stationary solutions. Thus, from Eq. (7), the Gauss law reads

$$\partial_i E_i - \kappa B = g^2 j_0, \tag{11}$$

with $j_0 = -\lambda^2 A_0(\vec{n}\cdot\partial_i\vec{\phi})^2$ being the electric charge density. The electric field is defined by $E_i = F_{0i} = -\partial_i A_0$ while the magnetic field is given by $B = F_{12} = \epsilon_{ij}\partial_i A_j$. The Gauss law shows the mixing of the electric and magnetic sectors, implying that the soliton solutions are carriers of both magnetic flux and electric charge.

Also, from Eq. (7), the stationary Ampère law gives

$$\partial_i B - \kappa E_i = -\lambda^2 g^2(\vec{n}\cdot\partial_i\vec{\phi})Q, \tag{12}$$

with $Q \equiv \vec{\phi}\cdot(D_1\vec{\phi}\times D_2\vec{\phi})$, which can still be expressed as

$$Q = \vec{\phi}\cdot(\partial_1\vec{\phi}\times\partial_2\vec{\phi}) + \epsilon_{ij}A_i(\vec{n}\cdot\partial_j\vec{\phi}). \tag{13}$$

The term $\vec{\phi}\cdot(\partial_1\vec{\phi}\times\partial_2\vec{\phi})$ is related to the topological charge or topological degree (also called the winding number) of the Skyrme field,

$$\deg[\vec{\phi}] = -\frac{1}{4\pi}\int d^2\mathbf{x}\,\vec{\phi}\cdot(\partial_1\vec{\phi}\times\partial_2\vec{\phi}) = k, \tag{14}$$

where $k \in \mathbb{Z}\backslash 0$.

Similarly, from Eq. (9), the stationary equation of motion of the Skyrme field becomes

$$\frac{\partial U}{\partial\phi_n}(\vec{n}\times\vec{\phi}) = \lambda^2\partial_i[(\vec{n}\cdot\partial_i\vec{\phi})(\Psi^2 - A_0^2)](\vec{n}\times\vec{\phi}) - \lambda^2\epsilon_{ij}D_i(QD_j\vec{\phi}). \tag{15}$$

In the next section, we will show how the BPS formalism is implemented. During the procedure, the self-dual potential $U(\phi_n,\Psi)$ is determined, allowing us to obtain the energy lower bound and the self-dual equations to be satisfied by the solitonic configurations saturating such a bound.

### A. The BPS structure

The stationary energy density of model (5) is

$$\epsilon = \frac{1}{2g^2}B^2 + \frac{1}{2g^2}(\partial_i A_0)^2 + \frac{\lambda^2}{2}(A_0)^2(\vec{n}\cdot\partial_i\vec{\phi})^2 + \frac{\lambda^2}{2}Q^2 + \frac{1}{2g^2}(\partial_i\Psi)^2 + \frac{\lambda^2}{2}\Psi^2(\vec{n}\cdot\partial_i\vec{\phi})^2 + U(\phi_n,\Psi), \tag{16}$$

where we have used $Q^2 = \frac{1}{2}(D_i\vec{\phi}\times D_j\vec{\phi})^2$. The requirement that the energy density be null when $|\vec{x}|\to\infty$ establishes the boundary conditions satisfied by the fields of the model.

The total energy is defined by integrating the energy density (16) so that the implementation of the BPS formalism allows us to write

$$E = \int d^2\mathbf{x}\left[\frac{1}{2g^2}(B\pm\Sigma)^2 + \frac{\lambda^2}{2}(Q\mp Z)^2 + \frac{1}{2g^2}(\partial_i A_0 \mp \partial_i\Psi)^2 + \frac{\lambda^2}{2}(A_0\mp\Psi)^2(\vec{n}\cdot\partial_i\vec{\phi})^2 \pm \lambda^2 A_0\Psi(\vec{n}\cdot\partial_i\vec{\phi})^2 \mp \frac{1}{g^2}B\Sigma - \frac{1}{2g^2}\Sigma^2 \pm \lambda^2 QZ - \frac{\lambda^2}{2}Z^2 \pm \frac{1}{g^2}(\partial_i A_0)\partial_i\Psi + U\right], \tag{17}$$

where we have introduced two auxiliary functions—namely, $\Sigma \equiv \Sigma(\phi_n,\Psi)$ and $Z \equiv Z(\phi_n)$—which we shall determine later. By using expression (13) and the Gauss law (11), we arrive at

$$E = \int d^2\mathbf{x}\left[\frac{1}{2g^2}(B\pm\Sigma)^2 + \frac{\lambda^2}{2}(Q\mp Z)^2 + \frac{1}{2g^2}(\partial_i A_0 \mp \partial_i\Psi)^2 + \frac{\lambda^2}{2}(A_0\mp\Psi)^2(\vec{n}\cdot\partial_i\vec{\phi})^2 \pm \lambda^2 Z\vec{\phi}\cdot(\partial_1\vec{\phi}\times\partial_2\vec{\phi}) \pm \frac{1}{g^2}\partial_i(\Psi\partial_i A_0) \mp \frac{1}{g^2}\epsilon_{ji}(\partial_j A_i)(\Sigma - \kappa\Psi) \pm \lambda^2\epsilon_{ij}A_i Z(\vec{n}\cdot\partial_j\vec{\phi}) - \frac{1}{2g^2}\Sigma^2 - \frac{\lambda^2}{2}Z^2 + U\right]. \tag{18}$$

At this point, we transform the fourth row of Eq. (18) into a total derivative. To achieve this, we first choose

$$\Sigma \equiv \lambda^2 g^2 W + \kappa\Psi, \tag{19}$$

where $W \equiv W(\phi_n)$. Thus, the fourth row in Eq. (18) results

$$\pm\lambda^2\epsilon_{ij}[(\partial_j A_i)W + A_i Z(\vec{n}\cdot\partial_j\vec{\phi})], \tag{20}$$

and it becomes a total derivative if $Z(\phi_n)$ is defined by

$$Z = \frac{\partial W}{\partial\phi_n}, \text{ such that } \partial_j W = \frac{\partial W}{\partial\phi_n}(\vec{n}\cdot\partial_j\vec{\phi}). \tag{21}$$

Therefore, the total energy becomes

$$E = \int d^2\mathbf{x}\Big\{\frac{1}{2g^2}[B \pm (\lambda^2 g^2 W + \kappa\Psi)]^2 + \frac{\lambda^2}{2}\left[Q \mp \frac{\partial W}{\partial \phi_n}\right]^2 + \frac{\lambda^2}{2}(A_0 \mp \Psi)^2(\vec{n}\cdot\partial_i\vec{\phi})^2 + \frac{1}{2g^2}(\partial_i A_0 \mp \partial_i\Psi)^2 \pm \lambda^2\left(\frac{\partial W}{\partial \phi_n}\right)\vec{\phi}\cdot(\partial_1\vec{\phi}\times\partial_2\vec{\phi}) \pm \frac{1}{g^2}\partial_i(\Psi\partial_i A_0) \mp \lambda^2\epsilon_{ij}\partial_j(A_i W) - \frac{1}{2g^2}(\lambda^2 g^2 W + \kappa\Psi)^2 - \frac{\lambda^2}{2}\left(\frac{\partial W}{\partial \phi_n}\right)^2 + U\Big\}. \quad (22)$$

To continue with the implementation of the BPS formalism, we require the potential $U(\phi_n, \Psi)$ to be defined as

$$U(\phi_n, \Psi) = \frac{\lambda^2}{2}\left(\frac{\partial W}{\partial \phi_n}\right)^2 + \frac{\lambda^4 g^2}{2}\left(W + \frac{\kappa}{\lambda^2 g^2}\Psi\right)^2. \quad (23)$$

Notably, $W(\phi_n)$ plays the role of a superpotential function, and it must be constructed (or proposed) such that the self-dual potential $U(\phi_n, \Psi)$ becomes null when $\phi_n \to 1$ (or $|\vec{x}| \to \infty$), in accordance with Eq. (16). Consequently, the following boundary conditions must be satisfied:

$$\lim_{\phi_n\to 1} W(\phi_n) = 0, \quad \lim_{\phi_n\to 1}\frac{\partial W}{\partial \phi_n} = 0, \quad \lim_{|\vec{x}|\to\infty}\Psi = 0. \quad (24)$$

Considering the boundary conditions (24), we observe the contributions of the total derivatives in the fourth row of Eq. (22) vanish. Therefore, we can express the total energy as

$$E = \bar{E} + E_{\mathrm{BPS}}, \quad (25)$$

where $\bar{E}$ represents the integral composed by the quadratic terms,

$$\bar{E} = \int d^2\mathbf{x}\Big\{\frac{1}{2g^2}[B \pm (\kappa\Psi + g^2\lambda^2 W)]^2 + \frac{\lambda^2}{2}\left[Q \mp \frac{\partial W}{\partial \phi_n}\right]^2 + \frac{1}{2g^2}(\partial_i A_0 \mp \partial_i\Psi)^2 + \frac{\lambda^2}{2}(A_0 \mp \Psi)^2(\vec{n}\cdot\partial_i\vec{\phi})^2\Big\}, \quad (26)$$

and $E_{\mathrm{BPS}}$ defines the energy lower bound,

$$E_{\mathrm{BPS}} = \pm\lambda^2\int d^2\mathbf{x}\left(\frac{\partial W}{\partial \phi_n}\right)\vec{\phi}\cdot(\partial_1\vec{\phi}\times\partial_2\vec{\phi}). \quad (27)$$

The total energy (25) satisfies the inequality

$$E \geq E_{\mathrm{BPS}} \quad (28)$$

because $\bar{E} \geq 0$. Then, the energy lower bound will be achieved when the fields possess configurations such that $\bar{E} = 0$, i.e., the bound is saturated when the following set of first-order differential equations are satisfied:

$$B = \mp g^2\lambda^2 W \mp \kappa\Psi, \quad (29)$$

$$Q = \pm\frac{\partial W}{\partial \phi_n}, \quad (30)$$

$$\partial_i\Psi = \pm\partial_i A_0, \qquad \Psi = \pm A_0. \quad (31)$$

These BPS configurations can be considered as classical solutions related to an extended supersymmetric theory [25] of the model (5). Indeed, such affirmation was shown in Ref. [17]; i.e., the BPS equations belong to an $\mathcal{N} = 2$ SUSY extension model whose bosonic sector would be given by the Lagrangian (5). Besides, the solutions of Eqs. (32)–(34) are type BPS 1/4, corresponding to the nontrivial phase of the $\mathcal{N} = 2$ SUSY extension model.

From Eq. (31), we observe that $\Psi = \pm A_0$ automatically satisfies both equations; consequently, the self-dual or BPS charged solitons are described by the equations

$$B = \mp g^2\lambda^2 W - \kappa A_0, \quad (32)$$

$$Q = \pm\frac{\partial W}{\partial \phi_n}, \quad (33)$$

together with the Gauss law (11),

$$\partial_i\partial_i A_0 + \kappa B = g^2\lambda^2 A_0(\vec{n}\cdot\partial_i\vec{\phi})^2. \quad (34)$$

A straightforward calculation shows that the Euler-Lagrange equations provided by the Lagrangian density (5) can be recovered starting from the set of BPS equations.

## III. ROTATIONALLY SYMMETRIC SKYRMIONS

We investigate solitons rotationally symmetric saturating the energy lower bound (27). Henceforth, without loss of generality, we set $\vec{n} = (0, 0, 1)$ such that $\phi_n = \phi_3$, and we assume the usual ansatz for the Skyrme field,

$$\vec{\phi}(r,\theta) = \begin{pmatrix} \sin f(r)\cos N\theta \\ \sin f(r)\sin N\theta \\ \cos f(r) \end{pmatrix}, \quad (35)$$

where $r$ and $\theta$ are polar coordinates, $N = \deg[\vec{\phi}]$ is the winding number introduced in Eq. (14), and $f(r)$ is a regular function satisfying the boundary conditions

$$f(0) = \pi, \qquad \lim_{r\to\infty} f(r) = 0. \tag{36}$$

We now introduce the field redefinition [13],

$$\phi_3 = \cos f \equiv 1 - 2h, \tag{37}$$

with the field $h = h(r)$ obeying

$$h(0) = 1, \qquad \lim_{r\to\infty} h(r) = 0. \tag{38}$$

For the gauge field $A_\mu$, we consider the ansatz

$$A_i = -\epsilon_{ij}x_j \frac{Na(r)}{r^2}, \qquad A_0 = \omega(r), \tag{39}$$

where $a(r)$ and $\omega(r)$ are well-behaved functions satisfying the boundary conditions

$$a(0) = 0, \qquad \lim_{r\to\infty} a(r) = a_\infty, \tag{40}$$

$$\omega(0) = \omega_0, \qquad \lim_{r\to\infty} \omega(r) = 0, \qquad \lim_{r\to\infty} \frac{d\omega}{dr} = 0, \tag{41}$$

where $a_\infty$ and $\omega_0$ are finite constants.

The superpotential $W(h)$ must satisfy

$$\lim_{r\to 0} W(h) = W_0, \qquad \lim_{r\to\infty} W(h) = 0, \qquad \lim_{r\to\infty} \frac{dW}{dh} = 0, \tag{42}$$

with the two last conditions having been obtained from Eq. (24). The constant $W_0$ is a positive-definite quantity.

The magnetic field and electric field are expressed as

$$B = \frac{N}{r}\frac{da}{dr}, \qquad E_r = -\frac{d\omega}{dr}. \tag{43}$$

whereas the BPS bound (27) becomes

$$E \geq E_{\mathrm{BPS}} = \pm 2\pi\lambda^2 N W_0. \tag{44}$$

As this is a positive-definite quantity, the sign $+(-)$ corresponds to $N > 0 (N < 0)$.

Similarly, the BPS equations and the Gauss law become

$$\frac{N}{r}\frac{da}{dr} + \lambda^2 g^2 W + \kappa\omega = 0, \tag{45}$$

$$\frac{4N}{r}(1+a)\frac{dh}{dr} + \frac{dW}{dh} = 0, \tag{46}$$

$$\frac{d^2\omega}{dr^2} + \frac{1}{r}\frac{d\omega}{dr} + \frac{\kappa N}{r}\frac{da}{dr} = 4\lambda^2 g^2 \omega \left(\frac{dh}{dr}\right)^2, \tag{47}$$

respectively. Furthermore, for the BPS energy density, we have

$$\epsilon_{\mathrm{BPS}} = \frac{B^2}{g^2} + \frac{1}{g^2}\left(\frac{d\omega}{dr}\right)^2 + 4\lambda^2\omega^2\left(\frac{dh}{dr}\right)^2 + \frac{\lambda^2}{4}\left(\frac{dW}{dh}\right)^2. \tag{48}$$

Note that in the BPS equations (45) and (46), without loss of generality, we have chosen the upper sign. Such an assumption will be considered in the remainder of the paper.

In the following sections, we study the behavior of the self-dual profiles at origin and in the limit $r \to \infty$ by solving the BPS equations (45) and (46) and the Gauss law (47).

### A. Behavior of the profiles at origin

We perform the analysis around the origin ($r = 0$) by using the boundary conditions previously defined and considering the superpotential $W(h)$ well-behaved function. Hence, we find the following behavior for the field profiles:

$$h(r) \approx 1 - \frac{(W_h)_{h=0}}{8N} r^2 + \frac{(W_h)_{h=0}(W_{hh})_{h=0}}{128N^2} r^4, \tag{49}$$

$$a(r) \approx -C_0 r^2 + C_1 r^4, \tag{50}$$

$$\omega(r) \approx \omega_0 + \frac{\kappa N C_0}{2} r^2 - \frac{\kappa N C_1}{4} r^4, \tag{51}$$

where $W_h = dW/dh$, $W_{hh} = d^2W/dh^2$, and the constants $C_0$, $C_1$ are defined as

$$C_0 = \frac{g^2\lambda^2 W_0 + \kappa\omega_0}{2N}, \tag{52}$$

$$C_1 = \frac{g^2\lambda^2 (W_h)^2_{h=0} - 4\kappa^2 N^2 C_0}{32N^2}. \tag{53}$$

The behaviors for magnetic and electric fields near the origin are

$$B(r) \approx -2NC_0 + 4NC_1 r^2, \tag{54}$$

$$E_r(r) \approx -\kappa N C_0 r + \kappa N C_1 r^3, \tag{55}$$

respectively, while the BPS energy density gives

$$\epsilon_{\mathrm{BPS}} \approx \frac{4N^2C_0^2}{g^2} + \frac{\lambda^2}{4}(W_h)_{h=0} + \left[\frac{3\kappa^2N^2C_0^2}{g^2} + \frac{\lambda^2(W_h)_{h=0}^2}{4N^2}\left(\omega_0^2 - 2N^2C_0 - \frac{N(W_{hh})_{h=0}}{4}\right)\right]r^2. \tag{56}$$

It is verified that the amplitude of the BPS energy density at the origin increases in accordance with the growth of the electromagnetic coupling $g$.

### B. Behavior of the profiles for large values of $r$

For our analysis in the asymptotic limit, $r \to \infty$, we consider a superpotential $W(h)$ behaving as

$$W(h) \approx W_\infty^{(\sigma)} h^\sigma, \tag{57}$$

where $W_\infty$ is a positive real constant and the parameter $\sigma \geq 2$. Under the boundary conditions, the asymptotic analysis leads us to two types of Skyrme field profiles: (i) for $\sigma = 2$, we have found soliton solutions whose tail decays following a Gaussian decay law, and (ii) for $\sigma > 2$, the profiles of the Skyrme field have a power-law decay. For both cases ($\sigma = 2$ and $\sigma > 2$), the gauge field profiles $a(r)$ and $\omega(r)$ decay following an exponential-law type.

#### 1. Behavior of the profiles for $\sigma = 2$

We select a superpotential whose behavior is

$$W(h) \approx W_\infty^{(2)} h^2, \tag{58}$$

such that the field profiles possess the following asymptotic behavior,

$$h(r) \approx C_\infty^{(h)} e^{-\Lambda r^2}, \tag{59}$$

$$a(r) \approx a_\infty - C_\infty \sqrt{r} e^{-\kappa r}, \tag{60}$$

$$\omega(r) \approx -C_\infty \frac{N}{\sqrt{r}} e^{-\kappa r}, \tag{61}$$

where the quantity $\Lambda$ has been defined as

$$\Lambda = \frac{W_\infty^{(2)}}{4N(1+a_\infty)}. \tag{62}$$

The finite constants $C_\infty^{(h)}$ and $C_\infty$ are fixed for every set of coupling constants and can be determined numerically. We note that the behavior shows explicitly that the Chern-Simons coupling constant $\kappa$ plays the role of the effective mass of the gauge field.

In addition, the magnetic and electric fields for large values of $r$ behave as

$$B(r) \approx C_\infty \frac{N\kappa}{\sqrt{r}} e^{-\kappa r}, \tag{63}$$

$$E_r(r) \approx -C_\infty \frac{N\kappa}{\sqrt{r}} e^{-\kappa r}, \tag{64}$$

respectively. We must highlight the behavior of the gauge field (including the ones for the electric and magnetic fields) resembles that of the Abrikosov-Nielsen-Olesen vortices arising in Abelian Higgs models [26]. The Maxwell-Higgs electrodynamics is the relativistic version of the Ginzburg-Landau theory of superconductivity, and the BPS limit of the Maxwell-Higgs model separates the superconducting phases type I and type II. Recently, similar gauge field behavior has also been found in other gauged Skyrme models [27,28].

#### 2. Behavior of the profiles for $\sigma > 2$

In this case, our analysis considers a superpotential behaving like Eq. (57) with $\sigma > 2$. Hence, when $r \to \infty$, the field profiles have the following asymptotic behavior:

$$h(r) \approx \left[\frac{8N(a_\infty+1)}{\sigma(\sigma-2)W_\infty^{(\sigma)}}\right]^{1/(\sigma-2)} \left(\frac{1}{r}\right)^{2/(\sigma-2)}, \tag{65}$$

$$a(r) \approx a_\infty - \mathcal{C}_\infty \sqrt{r} e^{-\kappa r}, \tag{66}$$

$$\omega(r) \approx -\mathcal{C}_\infty \frac{N}{\sqrt{r}} e^{-\kappa r}, \tag{67}$$

where $\mathcal{C}_\infty$ is a finite constant determined numerically.

We note that the profiles of the Skyrme field follow a power-law decay contrasting the behavior for $\sigma = 2$ given in Eq. (59). Field profiles following a power-law decay for large distances are called *delocalized*. This type of solution also arises in the study of fractional vortices in two-component superconductors [29], diamagnetic vortices in Chern-Simons theory [30], and in some $k$-generalized Abelian Higgs models [31]. On the other hand, the gauge field profiles $a(r)$ and $\omega(r)$ remain localized because they follow the same behavior of the ones analyzed in the previous case $\sigma = 2$, and, consequently, the magnetic and electric field behaviors are given by Eqs. (63) and (64), respectively.

## IV. NUMERICAL SOLUTIONS

### A. Numerical solutions for $\sigma = 2$

Our first numerical analysis is devoted to solve the BPS equations (45) and (46) and the Gauss law (47) by considering the superpotential

$$W(h) = \frac{h^2}{\lambda^2}, \tag{68}$$

where, without loss of generality, we have chosen $W_0 = W_\infty^{(2)} = 1/\lambda^2$. Thus, the BPS energy (44) is given by

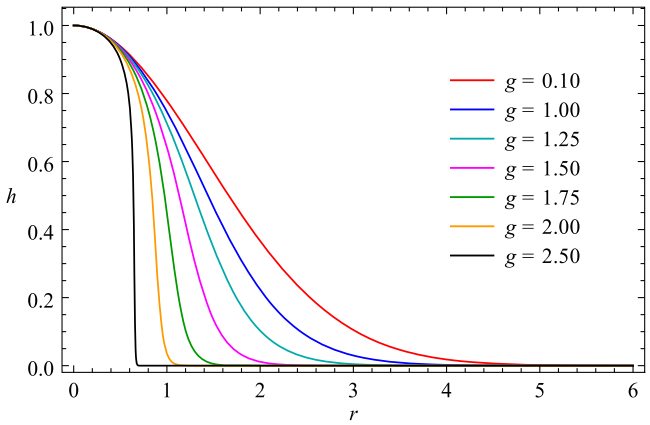


FIG. 1. Skyrme field profiles $h(r)$.

$$E_{\mathrm{BPS}} = \pm 2\pi N, \tag{69}$$

To solve the BPS equations, we set $N = 1$, $\lambda = 1$, $\kappa = 1$ and run the electromagnetic coupling constant $g$. The resulting solutions are shown in Figs. 1–6.

The profile functions $h(r)$ characterizing the Skyrme field are plotted in Fig. 1. Note that, for increasing values of $g$, the profiles become more localized around the origin. Also, for sufficiently large values of $g$ (in our analysis, $g \gtrsim 2.5$), the profiles rapidly attain the vacuum value, acquiring a structure resembling that of a compacton (a soliton of finite extent having its exact vacuum value outside of the compact region [32]). The arrival of the compactonlike structure is consistent with the behavior (59) of the Skyrme field profile which yields a fast exponential decay in the strong coupling limit of $g$, i.e., the parameter $\Lambda \to \infty$ as a consequence of $a_\infty \to -1$ (see Fig. 2).

Figure 2 depicts the vector potential profiles $a(r)$. Unlike the case of the uncharged BPS soliton solutions addressed in Ref. [13], here the vector potential profiles present an inverted ringlike shape (in our analysis, such a feature is better seen in the interval $0 < g < 2$) which goes vanishing for sufficiently large values of $g$, when the vector potential achieves a constant vacuum value $a_\infty \to -1$. Furthermore, as previously mentioned, when we have $a_\infty \to -1$, the soliton profiles become compactonlike structures. It is worth emphasizing that the appearance of ringlike structures is associated with the presence of a Chern-Simons term. In order to better visualize the ringlike effect for weak coupling, the profile for $g = 0.1$ (blue line) was rescaled by multiplying it by 100.

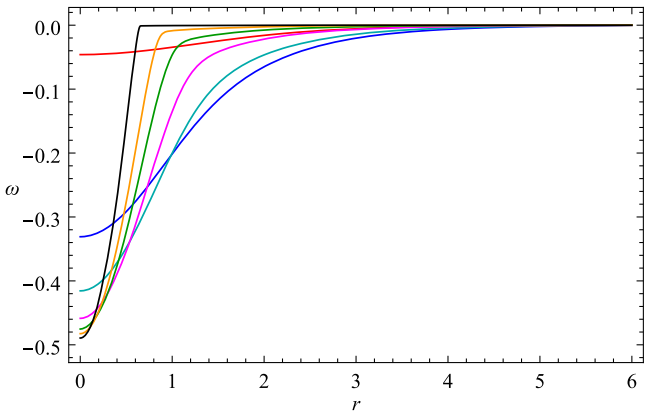


FIG. 3. Scalar potential $\omega(r)$. The profile for $g = 0.1$ (blue line) has been rescaled by multiplying it by 10. The conventions are as in Fig. 1.

The profiles for the scalar potential $\omega(r)$ and BPS energy density $\epsilon_{\mathrm{BPS}}(r)$ are shown in Figs. 3 and 4, respectively. In both cases, the amplitude at origin (in absolute value) increases with the growing of $g$. It is again observed that the profiles for sufficiently large values of $g$ present the compactlike format.

Additionally in Fig. 4, we have inserted the BPS energy density profiles for $N \geq 1$ ($g = 2.5$). The inset reveals that,

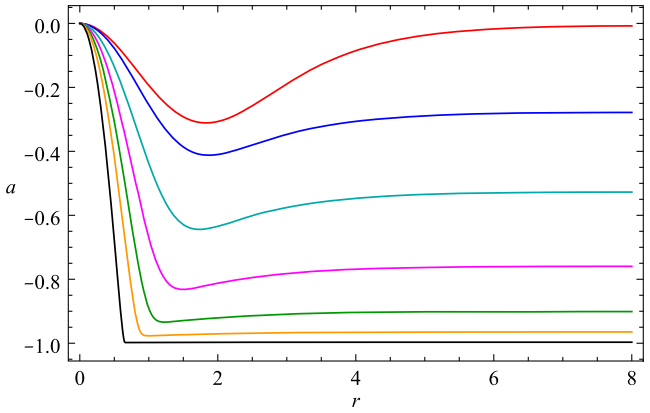


FIG. 2. Vector potential profiles $a(r)$. The profile for $g = 0.1$ (blue line) has been rescaled by multiplying by 100. The conventions are as in Fig. 1.

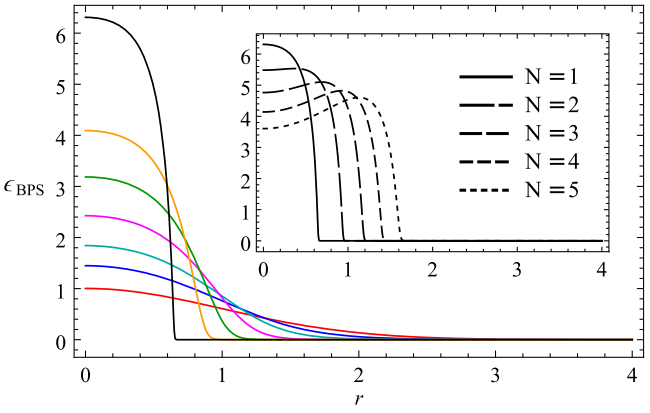


FIG. 4. BPS energy density $\epsilon_{\mathrm{BPS}}(r)$. The conventions are as in Fig. 1. (Inset) Profiles of $\epsilon_{\mathrm{BPS}}(r)$ for $N \geq 1$ with the electromagnetic coupling fixed at $g = 2.5$.

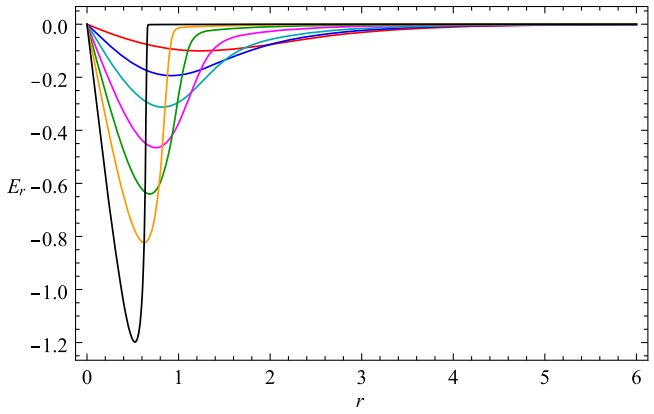


FIG. 5. Electric field $E_r(r)$. The profile for $g = 0.1$ (black dotted line) has been rescaled by multiplying it by 50. The conventions are as in Fig. 1.

for increasing values of $N$, the profiles acquire a more ringlike shape. Such an effect also happens in other Maxwell-Chern-Simons systems such as the Abelian Higgs model, gauge sigma model, or gauged $CP(2)$ model. Furthermore, it is worthwhile to comment that the magnetic field profiles also present a ringlike format for increasing values of $N$.

The profiles of the electric field $E_r(r)$ are present in Fig. 5. The profiles are rings whose maximum amplitude is localized closer to the origin as the coupling constant $g$ grows, acquiring a compactonlike form. Furthermore, we have done a rescaling (multiplying by 50) the profile for $g = 0.1$ (blue line) in order for the ring format to become more visible. The numerical solutions tell us that the electric field is negative for all values of $r$ and $g$.

Figure 6 depicts the profiles of the magnetic field $B(r)$ for a set of values of the coupling constant $g$. At first sight, we observe that whenever $g$ increases, the absolute value of the amplitude in $r = 0$ also increases. The profiles also become more localized around the origin, acquiring a compactonlike format. However, for sufficiently large values of $r$, an enlargement of the profiles (see the inset in Fig. 6) reveals a flip (sign inversion) of the magnetic field, which directly implies a localized magnetic flux inversion. Such a flip of the magnetic field becomes clearer in view of Eqs. (63) and (64). Given the behavior of the magnetic and electric fields, they tell us that, for large values of $r$, the fields have opposite signs. Thus, if the electric field is always negative, for large distances, the magnetic field will be positive. In our analysis, the maximum amplitude of the inversion grows in the interval of $0 < g \leq 1.2$; thereafter, it decreases continuously for $g > 1.2$ until it disappears for sufficiently large values of the coupling constant $g$. We highlight the fact that such a localized magnetic flux inversion in the present BPS model is a genuine effect due to presence of both the Maxwell and Chern-Simons terms once such an effect is absent when coupled separately with the Skyrme field [13,16].

The flip of the magnetic field is a peculiar phenomenon which also has been reported in some other $(2+1)$-dimensional systems. For example, such behavior arises in the study of two-component superconductors whose fractional vortices present a delocalized magnetic field [29]. It also occurs in some Lorentz-violating Maxwell-Higgs electrodynamics [22,33] and in a Lorentz-violating gauged $O(3)$ sigma model [23].

### B. Numerical solutions for $\sigma > 2$

Our second numerical analysis is performed by considering the superpotential

$$W(h) = \frac{h^\sigma}{\lambda^2}. \tag{70}$$

Similarly, we have chosen $W_0 = W_\infty^{(\sigma)} = 1/\lambda^2$. This way, the BPS energy (44) is given also by Eq. (69).

We have solved the set of equations (45)–(47) for different values of the parameter $\sigma$ by fixing $N = 1$,

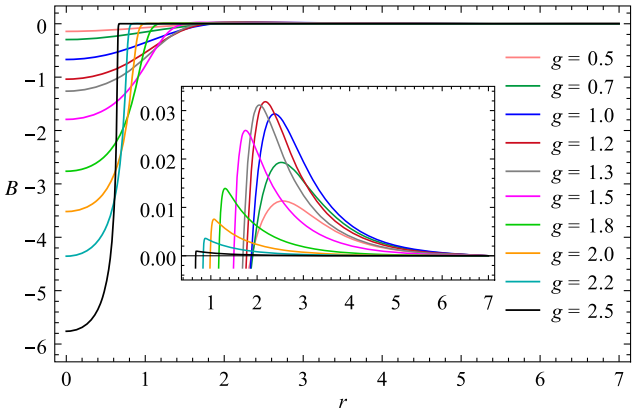


FIG. 6. Magnetic field $B(r)$. (Inset) Enlargement of the flip in the magnetic field.

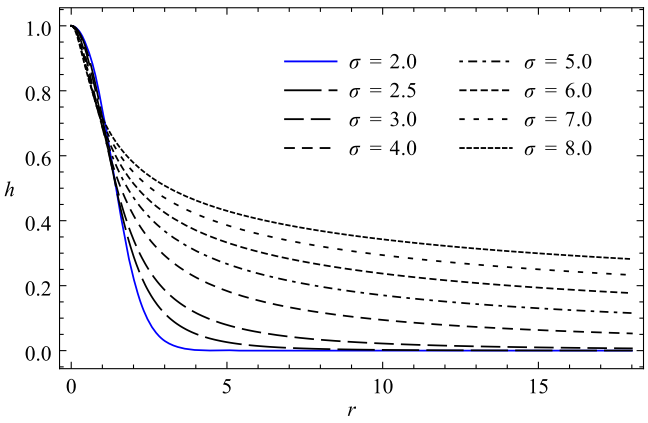


FIG. 7. Skyrme field profiles $h(r)$ for different values of $\sigma$ in superpotential (70).

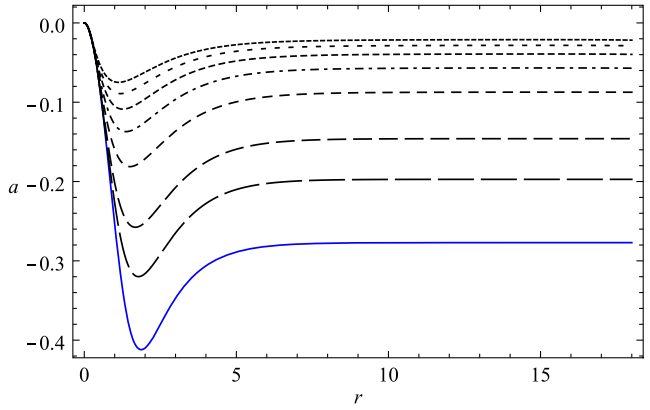


FIG. 8. Vector potential profiles $a(r)$. The conventions are as in Fig. 7.

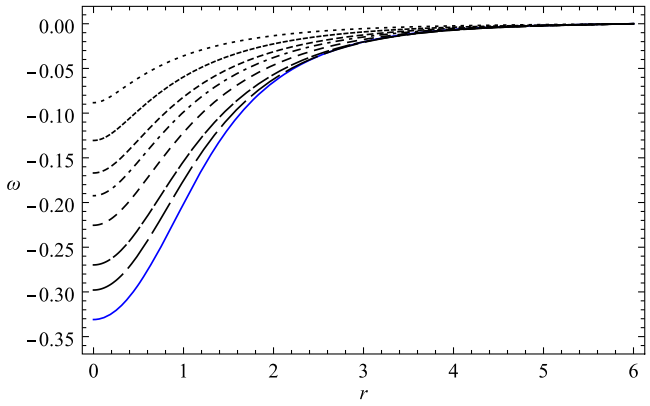


FIG. 9. Scalar potential $\omega(r)$. The conventions are as in Fig. 7.

$\lambda = 1$, $\kappa = 1$, $g = 1$. The numerical profiles are shown in Figs. 7–12.

Figure 7 shows clearly that for $\sigma > 2$ the Skyrme field profile $h(r)$ decays more slowly to its vacuum value whenever $\sigma$ increases, in accordance with the power law given in Eq. (65).

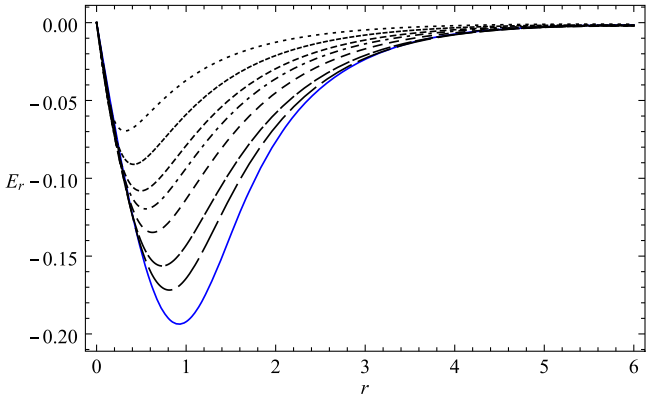


FIG. 10. Electric field $E_r(r)$. The conventions are as in Fig. 7.

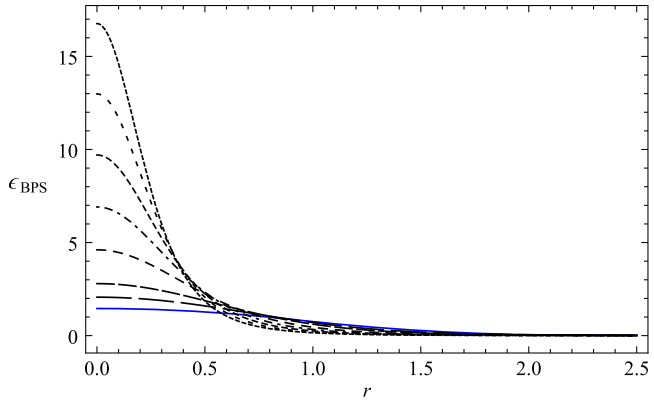


FIG. 11. BPS density energy $\epsilon_{\mathrm{BPS}}(r)$. The conventions are as in Fig. 7.

The general characteristics for profiles of the vector potential $a(r)$, scalar potential $\omega(r)$, electric field $E_r(r)$, self-dual energy density $\epsilon_{\mathrm{BPS}}(r)$, and magnetic field $B(r)$ are similar to the ones described in a previous section, but they become more and more localized near the origin with the growth of the parameter $\sigma$; see Figs. 8–12. Nevertheless, it is worthwhile to make some comments about the vector potential and magnetic field. In Fig. 8, we note the ringlike structures of the vector potential profiles are vanishing with an increase of $\sigma$, whereas $a(r)$ tends to zero. As a consequence of such behavior, the flip of the magnetic field is also present, and its maximum amplitude diminishes with an increase of $\sigma$; see Fig. 12.

### C. Magnetic flux and electric charge

The numerical results presented in the case of $\sigma = 2$ allow us to analyze important results about the magnetic flux and the total electric charge.

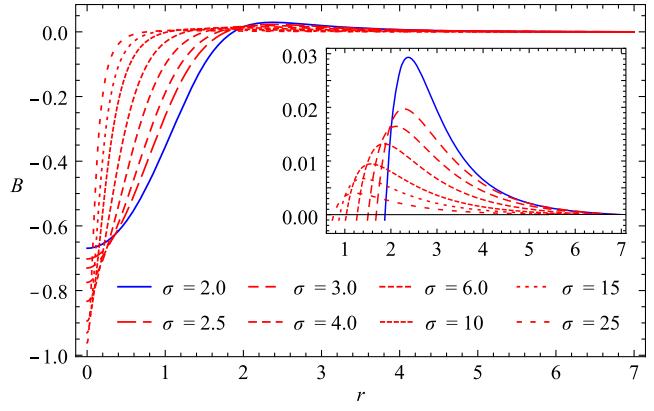


FIG. 12. Magnetic field $B(r)$ for other values of $\sigma$ in the superpotential (70). (Inset) Enlargement of the flip of the magnetic field for $\sigma \geq 2$.

The total magnetic flux is

$$\Phi = \int d^2\mathbf{x}\, B = 2\pi N a_\infty, \tag{71}$$

remembering that parameter $a_\infty$ is a finite real constant, in accordance with the boundary conditions established in Sec. III. Therefore, the magnetic flux is in general a nonquantized quantity (in the topological sense), unlike that belonging to the Chern-Simons Abelian Higgs models [34,35]. However, recent investigations have shown the existence of quantized magnetic flux in some Skyrme models [36].

By integrating the Gauss law (11), we compute the total electric charge in terms of the magnetic flux,

$$\mathcal{Q}_{\rm em} = \int d^2\mathbf{x} j_0 = -\frac{\kappa}{g^2}\Phi = -\frac{2\pi\kappa}{g^2} N a_\infty, \tag{72}$$

showing that it is nonquantized, too.

We observe, in the description of Fig. 2, that, for a sufficiently strong coupling $g$, the vacuum value of the potential vector $a_\infty \to -1$, which implies that the magnetic flux (71) becomes quantized in this limit. Such behavior of the magnetic flux profiles for $N = 1$ (black dotted line) and $N = 2$ (red dotted line) is depicted in Fig. 13. This effective quantization implies that the total electric charge (72) also becomes quantized in such a regime.

Figure 14 exhibits the behavior of the total electric charge as a function of the coupling constants $g$ [$\mathcal{Q}_{\rm em}(g)$ with $\kappa$ fixed] and $\kappa$ [$\mathcal{Q}_{\rm em}(\kappa)$ with $g$ fixed] by adopting the superpotential (68) with $\lambda = 1$. For the first analysis, we fixed $\kappa = 1$. We note that the total electric charge $\mathcal{Q}_{\rm em}(g)$ increases in accordance with $g$, achieving a maximum value at $g_{\rm max} \simeq 1.387$ for $N = 1$ (green dotted line) after the electric charge diminishes when $g$ increases continuously, i.e., $\mathcal{Q}_{\rm em}(g) \sim g^{-2}$ for $g \gg g_{\rm max}$, which is compatible with Eq. (72).

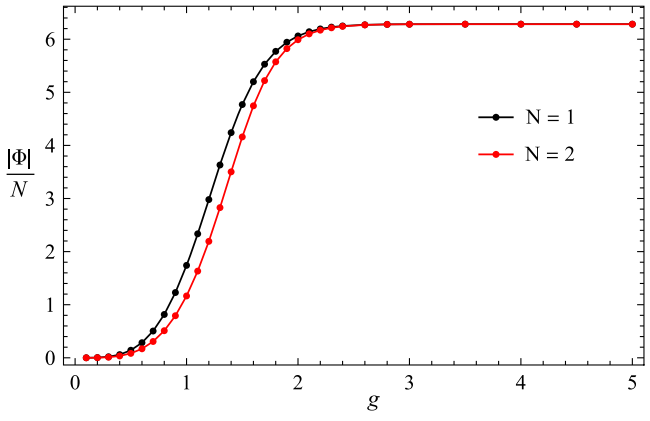


FIG. 13. The magnetic flux $|\Phi|$ in units of $N$ as a function of the gauge coupling $g$ for the superpotential (68) with fixed values $\lambda = 1$ and $\kappa = 1$.

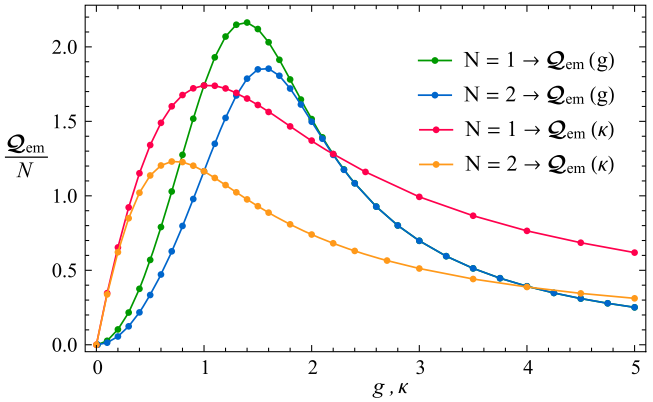


FIG. 14. The total electric charge in units of $N$ as a function of both the constant electromagnetic coupling $\mathcal{Q}_{\rm em}(g)$ and Chern-Simons coupling $\mathcal{Q}_{\rm em}(\kappa)$ for the superpotential (68) with $\lambda = 1$.

The second analysis presented in Fig. 14 is performed by considering the gauge coupling constant fixed at $g = 1$. We observe that the total electric charge $\mathcal{Q}_{\rm em}(\kappa)$ grows as $\kappa$ does and reaches a maximum value at $\kappa_{\rm max} \simeq 1.045$ for $N = 1$ (red dotted line). From then on, it gradually lessens with the continuous growth of the Chern-Simons coupling. Although that behavior is not directly explained by Eq. (72), we find numerically that, for the interval $0 < \kappa < \kappa_{\rm max}$, the vacuum value $a_\infty$ seems to grow linearly with $\kappa$; see Fig. 15. For $\kappa > \kappa_{\rm max}$, the values of $a_\infty$ increase slower than the growth of coupling $\kappa$; this behavior can be better understood by analyzing the inset of Fig. 15, where we have $\ln|a_\infty|$ as a function of $\ln\kappa$. We note that $|a_\infty| \sim \kappa^{-2}$ for $\kappa \gg \kappa_{\rm max}$.

Now let us briefly comment on the magnetic flux and total electric charge for the case where $\sigma > 2$. In Fig. 8, we note that, for a fixed value of the gauge coupling $g$, the vacuum value $a_\infty$ goes to zero continuously as $\sigma$ grows, i.e., $\lim_{\sigma\to\infty} a_\infty = 0$. Consequently, the magnetic flux and the

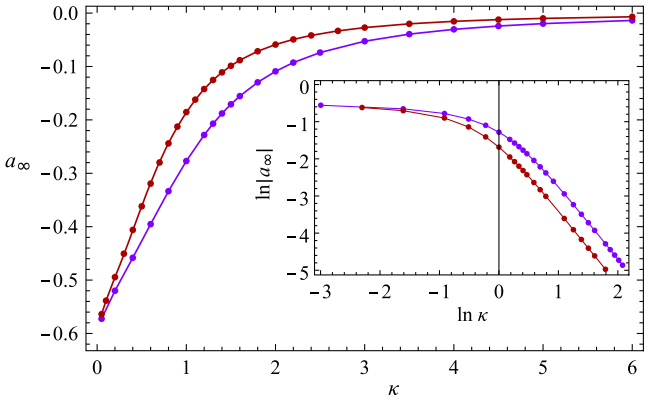


FIG. 15. The gauge vacuum value $a_\infty$ as a function of the Chern-Simons coupling $\kappa$ when assuming the superpotential (68) with $g = 1$, $\lambda = 1$. We have depicted $N = 1$ (violet dotted line) and $N = 2$ (dark red dotted line). (Inset) Logarithm of the absolute value of $a_\infty$ as a function of the logarithm of $\kappa$.

total electric charge become null. An analogous result also was obtained in the generalized Chern-Simons baby Skyrme model [16].

## V. CONCLUSIONS AND REMARKS

In this paper, we show the existence of BPS charged configurations in a gauged baby Skyrme model (5) whose gauge field is governed by the Maxwell-Chern-Simons action. The BPS model (5) is constructed by introducing a scalar field $\Psi$ into model (2) which couples adequately to the Skyrme field $\vec{\phi}$ but does not couple to the gauge field. The successful implementation of the BPS technique allows us to obtain the Bogomol'nyi bound (related to the topological charge of the Skyrme field), and hence the self-dual or BPS equations whose solutions saturate this bound. We point out that the introduction of a superpotential function determining the self-dual potential is an important step in the successful implementation of the BPS technique. Such a superpotential is considered to be a well-behaved function in the whole target space and plays an important role in defining the BPS configurations.

With the aim of studying the properties of self-dual configurations, we use a rotationally symmetric ansatz. Thus, it is verified that the total energy (44) is topologically quantized because it is proportional to the topological charge $N$ of the Skyrme field. Next, we analyze the asymptotic behavior ($r \to \infty$) of the solutions by choosing a superpotential function that in such a limit behaves as $W(h) \approx h^{\sigma}/\lambda^2$. It allows us to find two types of self-dual profiles for the Skyrme field. The first one was obtained for $\sigma = 2$, providing solutions whose tail decays following a Gaussian law $e^{-\Lambda r^2}$, with $\Lambda$ given in Eq. (62). The second type occurs for $\sigma > 2$, solutions whose tail decays following a power law $r^{-\beta(\sigma)}$, with $\beta(\sigma) = 2/(\sigma - 2)$; see Eq. (65). For both types of skyrmion profiles, the respective gauge fields possess an exponential-law type $e^{-\kappa r}$ (i.e., the Chern-Simons coupling constant becomes the gauge field mass), very similar to behavior found for such fields in Abelian Higgs models describing Abrikosov-Nielsen-Olesen vortices.

Next, we dedicate our effort to solve numerically the differential equations describing the BPS configurations in order to attain the main properties or characteristics. For such a purpose, we consider the superpotential defined by $W(h) = h^{\sigma}/\lambda^2$ and study the solitons for $\sigma \geq 2$. We show that the soliton profiles exhibit a compactonlike format for sufficiently large values of the electromagnetic coupling constant $g$. Furthermore, the soliton solutions carry magnetic flux and possess nonzero total electric charge, and, although both of them are proportional to the winding number $N$, they are nonquantized quantities because the vacuum value $a_{\infty}$ is a noninteger [see Eqs. (71) and (72), respectively]. However, it is shown numerically that, for sufficiently large values of the electromagnetic coupling $g$, the vacuum value $a_{\infty} \to -1$; thus, both quantities become effectively quantized, in accordance with previous investigations [13,16,37].

The more remarkable property is the emergence of the flip of the magnetic field, resulting in a localized magnetic flux inversion. This interesting feature emerges due to the presence of both Maxwell and Chern-Simons terms in the BPS model (5). We emphasize that such a feature is absent from previous investigations of gauged restricted baby Skyrme models with the Maxwell term [13] or the Chern-Simons term [16] alone.

It is worthwhile to point out the deep connection that has already been established between theories with extended supersymmetry and BPS structures [25]. In this sense, supersymmetry has provided us with a better understanding of the BPS sectors of some Skyrme models; see, e.g., Refs. [17,38,39]. In particular, the BPS structure obtained from model (5) has a close relation with the correspondent BPS sector of a $\mathcal{N} = 2$ SUSY extension model studied in Ref. [17].

We now are investigating the existence of BPS solitons in gauged baby Skyrme models in the presence of Lorentz violation. The results will be reported elsewhere.

## ACKNOWLEDGMENTS

This study was financed in part by the Coordenação de Aperfeiçoamento de Pessoal de Nível Superior–Brasil (CAPES), Finance Code No. 001. We thank the Conselho Nacional de Desenvolvimento Científico e Tecnológico (CNPq) and the Fundação de Amparo à Pesquisa e ao Desenvolvimento Científico e Tecnológico do Maranhão (FAPEMA) (Brazilian Government agencies). In particular, A. C. S., C. F. F., and A. L. M. acknowledge the full support of CAPES. R. C. acknowledges support from Grants No. CNPq/306385/2015-5, No. CNPq/423862/2018-9, and No. FAPEMA/Universal-01131/17.

[1] T. H. R. Skyrme, Proc. R. Soc. London **260**, 127 (1961); Nucl. Phys. **31**, 556 (1962); J. Math. Phys. (N.Y.) **12**, 1735 (1971).
[2] G. S. Adkins, C. R. Nappi, and E. Witten, Nucl. Phys. **B228**, 552 (1983); G. S. Adkins and C. R. Nappi, Nucl. Phys. **B233**, 109 (1984); C. J. Halcrow, C. King, and N. S. Manton, Phys. Rev. C **95**, 031303(R) (2017); C. Naya and P. Sutcliffe, Phys. Rev. Lett. **121**, 232002 (2018); I. Sharma, R. Kumar, and M. K. Sharma, Nucl. Phys. **A983**, 276 (2019).

[3] G. E. Volovik, *Exotic Properties of Superfluid $^3$He* (World Scientific, Singapore, 1992); *The Universe in a Helium Droplet* (Oxford University Press, New York, 2009).

[4] S. L. Sondhi, A. Karlhede, S. A. Kivelson, and E. H. Rezayi, Phys. Rev. B **47**, 16419 (1993); O. Schwindt and N. R. Walet, Europhys. Lett. **55**, 633 (2001); A. C. Balram, U. Wurstbauer, A. Wojs, A. Pinczuk, and J. K. Jain, Nat. Commun. **6**, 8981 (2015); T. Chen and T. Byrnes, Phys. Rev. B **99**, 184427 (2019).

[5] U. Al Khawaja and H. Stoof, Nature (London) **411**, 918 (2001); H. Luo, L. Li, and W. Liu, Sci. Rep. **9**, 18804 (2019).

[6] J. Fukuda and S. Žumer, Nat. Commun. **2**, 246 (2011).

[7] S. Mühlbauer, B. Binz, F. Jonietz, C. Pfleiderer, A. Rosch, A. Neubauer, R. Georgii, and P. Boni, Science **323**, 915 (2009); X. Z. Yu, Y. Onose, N. Kanazawa, J. H. Park, J. H. Han, Y. Matsui, N. Nagaosa, and Y. Tokura, Nature (London) **465**, 901 (2010); T. Dohi, S. DuttaGupta, S. Fukami, and H. Ohno, Nat. Commun. **10**, 5153 (2019).

[8] U. K. Rößler, A. N. Bogdanov, and C. Pfleiderer, Nature (London) **442**, 797 (2006); A. A. Zyuzin, J. Garaud, and E. Babaev, Phys. Rev. Lett. **119**, 167001 (2017); S. M. Dahir, A. F. Volkov, and I. M. Eremin, Phys. Rev. Lett. **122**, 097001 (2019).

[9] A. V. Shurgaia, H. J. W. Müller-Kirsten, and D. H. Tchrakian, Ann. Phys. (N.Y.) **228**, 146 (1993); B. M. A. G. Piette, B. J. Schroers, and W. J. Zakrzewski, Nucl. Phys. **B439**, 205 (1995); S. Bolognesi and W. Zakrzewski, Phys. Rev. D **91**, 045034 (2015).

[10] R. H. Hobart, Proc. Phys. Soc. London **82**, 201 (1963); G. H. Derrick, J. Math. Phys. (N.Y.) **5**, 1252 (1964).

[11] T. Gisiger and M. B. Paranjape, Phys. Rev. D **55**, 7731 (1997).

[12] C. Adam, T. Romanczukiewicz, J. Sanchez-Guillen, and A. Wereszczynski, Phys. Rev. D **81**, 085007 (2010).

[13] C. Adam, C. Naya, J. Sanchez-Guillen, and A. Wereszczynski, Phys. Rev. D **86**, 045010 (2012).

[14] C. Adam, C. Naya, T. Romanczukiewicz, J. Sanchez-Guillen, and A. Wereszczynski, J. High Energy Phys. 05 (2015) 155.

[15] C. Adam, C. Naya, J. Sanchez-Guillen, and A. Wereszczynski, J. High Energy Phys. 03 (2013) 012.

[16] R. Casana, A. C. Santos, C. F. Farias, and A. L. Mota, Phys. Rev. D **100**, 045022 (2019).

[17] J. M. Queiruga, J. Phys. A **52**, 055202 (2019).

[18] C. K. Lee, K. M. Lee, and H. Min, Phys. Lett. B **252**, 79 (1990).

[19] B. H. Lee, C. K. Lee, and H. Min, Phys. Rev. D **45**, 4588 (1992).

[20] S. Bolognesi and S. B. Gudnason, Nucl. Phys. **B805**, 104 (2008).

[21] K. Kimm, K. Lee, and T. Lee, Phys. Rev. D **53**, 4436 (1996).

[22] R. Casana, M. M. Ferreira, Jr., E. da Hora, and C. Miller, Phys. Lett. B **718**, 620 (2012); R. Casana and G. Lazar, Phys. Rev. D **90**, 065007 (2014).

[23] R. Casana, C. F. Farias, and M. M. Ferreira, Jr., Phys. Rev. D **92**, 125024 (2015).

[24] R. Casana, C. F. Farias, M. M. Ferreira, Jr., and G. Lazar, Phys. Rev. D **94**, 065036 (2016).

[25] E. Witten and D. Olive, Phys. Lett. **78B**, 97 (1978); Z. Hlousek and D. Spector, Nucl. Phys. **B370**, 143 (1992).

[26] A. A. Abrikosov, Zh. Eksp. Teor. Fiz. **32**, 1442 (1957) [Sov. Phys. JETP **5**, 1174 (1957)]; H. B. Nielsen and P. Olesen, Nucl. Phys. **B61**, 45 (1973).

[27] A. Yu. Loginov, J. Exp. Theor. Phys. **118**, 217 (2014).

[28] F. Navarro-Lérida and D. H. Tchrakian, Phys. Rev. D **99**, 045007 (2019).

[29] E. Babaev, J. Jaykka, and M. Speight, Phys. Rev. Lett. **103**, 237002 (2009).

[30] M. M. Anber, Y. Burnier, E. Sabancilar, and M. Shaposhnikov, Phys. Rev. D **92**, 085049 (2015).

[31] R. Casana, A. Cavalcante, and E. da Hora, J. High Energy Phys. 12 (2016) 051.

[32] T. Gisiger and M. B. Paranjape, Phys. Rev. D **55**, 7731 (1997).

[33] R. Casana, M. M. Ferreira, Jr., E. da Hora, and A. B. F. Neves, Eur. Phys. J. C **74**, 3064 (2014).

[34] S. K. Paul and A. Khare, Phys. Lett. B **174**, 420 (1986).

[35] H. J. de Vega and F. A. Schaposnik, Phys. Rev. Lett. **56**, 2564 (1986).

[36] C. Adam and A. Wereszczynski, Phys. Rev. D **95**, 116006 (2017); A. Samoilenka and Y. Shnir, Phys. Rev. D **97**, 045004 (2018).

[37] J. Gladikowski, B. M. A. G. Piette, and B. J. Schroers, Phys. Rev. D **53**, 844 (1996).

[38] M. Nitta and S. Sasaki, Phys. Rev. D **90**, 105002 (2014); **91**, 125025 (2015); S. B. Gudnason, M. Nitta, and S. Sasaki, J. High Energy Phys. 01 (2017) 014.

[39] C. Adam, J. M. Queiruga, J. Sanchez-Guillen, and A. Wereszczynskic, J. High Energy Phys. 05 (2013) 108; J. M. Queiruga, Phys. Rev. D **92**, 105012 (2015).